Thin Solid Films 722 (2021) 138574

Contents lists available at ScienceDirect

Thin Solid Films

journal homepage: www.elsevier.com/locate/tsf

Spontaneous fluctuations in a plasma ion assisted deposition – correlation between deposition conditions and vanadium oxide thin film growth

Anna Frank [a,*], Miguel Dias [b], Stefan Hieke [a], Angela Kruth [b], Christina Scheu [a,c,*]

[a] Max-Planck-Institut für Eisenforschung GmbH, Nanoanalytics and Interfaces, Max-Planck-Straße 1, 40237 Düsseldorf, Germany
[b] Leibniz Institute for Plasma Science and Technology e.V. (INP), Felix-Hausdorff-Straße 2, 17489 Greifswald, Germany
[c] Materials Analytics, RWTH Aachen University, Kopernikusstraße 10, 52074 Aachen, Germany

ARTICLE INFO

Keywords:
Transmission electron microscopy
Plasma assisted deposition
Deposition control
Vanadium oxide

ABSTRACT

In this work correlations between thin film crystallinity of plasma ion assisted electron beam evaporated vanadium oxide (VO_x) and fluctuations of the deposition parameters during the growth process could be observed by *in situ* monitoring deposition conditions and electron microscopy studies. In the presented case, unintentional fluctuations in the gas flow at the plasma source caused by inhomogeneous melting of the target material lead to an increase in discharge current and therefore a decrease of the oxygen flow in the plasma source, resulting in the formation of highly crystalline bands due to a temporary increase in energy flux. The major part of the VO_x thin film consists of a large number of nanocrystals embedded in an amorphous phase. In-depth structural analysis confirms a mixture of V_2O_5, in different modifications, VO_2, as well as the mixed-valence oxides V_4O_9 and V_6O_{13}, for nanocrystalline parts and crystalline bands. These differ mainly in the degree of crystallinity being influenced by variations in discharge current, and partly in the amount of higher oxidized vanadium oxides. In future, precisely controlled variation of plasma source conditions will open up pathways to control and tailor crystallinity of electron beam evaporated thin films, allowing for production methods for patterned thin films or layers with graduated crystallinity. This may give rise to a new class of coatings of nanohybrids combining amorphous VO_x with low electrical conductivity and crystalline domains providing a higher electrical conductivity which is useful for electrochromic displays, smart windows, and solar cells.

1. Introduction

In the light of recent tremendous research interest in the development of nanostructured materials, innovative concepts for new materials but also new synthesis approaches are needed. Traditional methods for industrial production of thin layers such as printing of wet-chemical precursors are often limited in terms of precise tailoring of microstructure and definition of crystallinity at a local scale.

Plasma assisted processes offer the advantage of allowing for unusual reaction pathways in deposition processes such as electron beam evaporation, adding new means of structure control by delivering additional energy and charge carried during the deposition process. Another advantage is that deposition temperatures are in general low, opening up the range of substrate materials that may be employed. For instance, crystalline thin metal oxide layers can be deposited by plasma ion assisted electron beam evaporation (PIAD) at comparable low temperatures of around 200°C onto carbon, glass, or polymeric support materials [1].

However, plasma processes are still not well understood and links between deposition parameters and properties of the as-grown films have to be established. One powerful technique to investigate local changes in crystallinity and chemical composition is (scanning) transmission electron microscopy ((S)TEM) which allows characterization down to the atomic scale. In this work, we will bridge this gap by studying the effect of variations in the PIAD conditions during growth on the local crystalline structure of vanadium oxides. As a case study, unintentional changes in the discharge current are correlated to the associated changes in the crystallinity, crystal structure, and chemical composition within the as-deposited film.

Vanadium oxides show rich redox chemistry due to their variable oxidation state which opens up a wide range of applications. Vanadium can adopt various oxidation states, ranging from +I to +V, giving rise to a large number of various vanadium oxides such as V_2O, VO, V_2O_3, VO_2, V_2O_5, and related intergrown structures with mixed valencies, for

* Corresponding authors.
E-mail addresses: frank@mpie.de (A. Frank), scheu@mpie.de (C. Scheu).

https://doi.org/10.1016/j.tsf.2021.138574
Received 31 October 2019; Received in revised form 4 February 2021; Accepted 4 February 2021
Available online 7 February 2021

example, V_6O_{13} and V_4O_9 [2]. Mostly, they are composed of vanadium oxide octahedra which share edges, corners, or even faces [2]. Since they possess either layered or open structures, vanadium oxides are also interesting as cathode materials in ion battery applications [2–4] but also for photocatalytic applications [5,6]. Vanadium pentoxide (V_2O_5) on the other hand, also is a main candidate material for electrochromic windows. Low-cost production of durable uniform coatings of V_2O_5 without pinholes or gaps becomes more significant with the ever-growing demand for such energy-saving *green* technologies [7].

Because of their general similarity, different structure types of nanocrystalline vanadium oxides are often very difficult to distinguish by X-ray or electron diffraction techniques due to the dominance of very similar *d*-values. Absolute quantification of oxygen from energy-dispersive X-ray (EDX) spectroscopy is challenging. One approach, however, is the application of experimental k-factors which can be obtained from a standard material with well-known V-to-O composition. The Cliff-Lorimer equation [8] (Eq. (1)) for binary compounds

$$\frac{C_a}{C_b} = k_{a,b}\frac{I_a}{I_b} \tag{1}$$

sets the weight percent C_a and C_b of the respective elements A and B into relation to the spectral intensities I_a and I_b by using the factor $k_{a,b}$. The k-factor is a sensitivity factor and not a constant, varying with the EDX system, the used acceleration voltage, and also effects like fluorescence, absorption, and the atomic number *Z* of the element(s) [9]. Measurement on a standard material with known composition, *i.e.* C_a:C_b ratio, allows calculating the sensitivity factor for the specific material and settings. This factor can then be used to quantify samples of the same elements but with unknown composition. However, EDX is not giving information about the oxidation state of the elements.

Electron energy loss spectroscopy (EELS) performed in STEM can be used to determine the oxidation state of vanadium by analysing differences in the energy loss near edge structure (ELNES) in the O K and V $L_{2,3}$ element-specific edges. From this fingerprint analysis, conclusions on the structure type of vanadium oxide and its oxidation state can be drawn, without the need of quantifying the element-specific edges [10,11].

In this work, we use a PIAD process for growing vanadium oxide thin films on silicon substrates. The flux of oxygen is monitored continuously during the deposition, as well as the discharge current, deposition rate, and film thickness. In combination with electron microscopic techniques, insights into the correlation between unintentional changes of deposition parameters and quality of the thin film are gained. A strong impact on crystallinity, and also partly onto crystal structure and chemical composition of the deposited films is observed. The obtained knowledge can be used in the future for tailoring thin film growth by adjusting the plasma parameters accordingly.

2. Materials and methods

2.1. Deposition of vanadium oxide thin films

VO_x thin layer samples with a nominal thickness of 500 nm were prepared by PIAD in a Marquis M900 coating chamber with a schematic sketch presented in Fig. 1. The chamber contained an approximate volume of 1 m^3 and is equipped with an end Hall ion source [12] with a hollow cathode used as an electron source. A vanadium metal target was evaporated by means of an electron beam gun (EBG) located next to the ion source. The EBG was equipped with a separate oxygen source allowing for direct control of the oxygen flux by the evaporation parameter.

The ion source was operated at an argon flow fixed at 10 SCCM plus a variable flow of oxygen, defined by the discharge voltage (V_d) and discharge current (I_d) of the plasma source, in addition an oxygen flow of 30 SCCM is provided directly to the EBG. For the presented sample a discharge voltage of 100 V and discharge current of 6 A were used, meaning an oxygen flow of 32.5 SCCM in the plasma source.

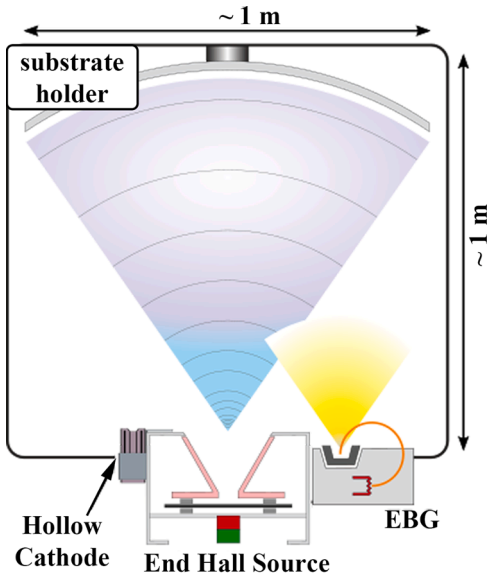

Fig. 1. Schematic drawing of the Marquis M900 coating chamber with end Hall ion source.

The substrate holder was positioned at the top of the chamber and rotated at a constant speed of 30 rotations/minute during deposition to ensure uniform coating. Single-crystalline silicon (Si) wafers with a [100] crystal orientation, without removal of the native oxide, were used as substrates, exhibiting a geometric size of 2.5 cm x 2.5 cm and a thickness of 500 µm (MicroChemicals GmbH).

The sample discussed in this work was deposited at a substrate temperature of 150°C and a deposition rate of 0.2 nm/s. The nominal thickness of the film was 500 nm, controlled by a quartz crystal microbalance. During the deposition, the gas flow of the plasma source, the discharge current, film thickness, and deposition rate were automatically recorded.

2.2. Characterization

The global crystal structure of the thin film was firstly characterized by grazing incidence X-ray diffraction (GIXRD). The measurements were performed using a Bruker D8 Advance XRD with a copper X-ray source (Cu Kα, 40 kV, 40 mA) in grazing incidence configuration and a LYNXEYE XE-T detector. The samples were measured at an incidence angle ω of 0.5° over a range of 2θ between 10° and 100°, at a step width of 0.02° and with data collected at 5 s/step.

Sample preparation for (S)TEM was carried out by focused ion beam (FIB), following the conventional lift-out technique [13] but using modified settings which have already been successfully applied in the preparation of cross-sectional samples from various thin films [14–16]. First, a protective platinum coating was deposited on top of the film assisted by an electron beam operated at 5 kV and 2.7 nA, followed by a second layer where a gallium beam is used to deposit platinum at 30 kV and 48 pA. Second, the surrounding material was removed by means of a gallium beam at 30 kV and a current of 6.5 nA. Third, the lamella was lifted out, using a Kleindiek micromanipulator, and transferred to a copper support grid. Finally, the lamella was thinned to electron transparency by varying the energy and beam current of the gallium beam ions from 30 kV to 16 kV and 0.7 nA down to 50 pA, while lowering the incident angle of the gallium beam to the lamella respectively.

(S)TEM investigations were performed on two ThermoScientific Titan Themis 300 (S)TEM instruments, both operated at an acceleration voltage of 300 kV. One (S)TEM instrument was equipped with a C_S probe

corrector and a Gatan Quantum ERS energy filter, while the other (S) TEM was in possession of a C_S image corrector. At both machines, a Bruker Super X-EDX detector was attached. Calibration for electron diffraction patterns was carried out by determining the camera constant via measurements and analysis of electron diffraction data of the Si substrate. The data of the film was then evaluated and compared to literature data [17]. Dual EELS was conducted at a dispersion of 0.1 eV and a spectral resolution of 1 eV. STEM images were acquired using the attached high angle annular dark field (HAADF) detector and collection angles of 78 to 200 mrad.

Quantitative EDX analysis was performed with the help of the Bruker Esprit 1.9.4 software. Measurements on a V_2O_5 standard material, which was checked on phase purity by XRD before, were performed to obtain an experimental $k_{V,O}$-factor. The $k_{V,O}$-factor was calculated using the following equation [8]:

$$k_{V,O} = \frac{C_V}{C_O}\frac{I_O}{I_V} = \frac{2}{5}\frac{I_O}{I_V} \quad (2)$$

The $k_{V,O}$-factor is 0.44 ± 0.04 and was used to quantify the EDX results. The obtained weight percent ratios were converted into atomic percent ratios and then compared to the theoretical V-to-O ratios of the different vanadium oxides, ranging from 0.40 for V_2O_5, over 0.44 (V_4O_9), and 0.46 (V_6O_{13}), 0.50 (VO_2), to 0.67 for V_2O_3. This way, changes in the chemical composition at different locations are analyzed.

3. Results and discussion

During normal operation of the PIAD process, several operating parameters are automatically tracked for quality and process monitoring. Among the data collected, the user has access to the applied voltage V_d, discharge current I_d, gas flow on the plasma source, deposition rate, and film thickness over time. For a given deposition, the user chooses V_d and I_d values, with the gas flow on the source being automatically defined by the system depending on the value of I_d. During the deposition process, in the eventuality of a change in measured I_d, the system reacts automatically and adjusts the gas flow in accordance until the user-defined value for I_d is achieved again. The deposition rate, also user-defined, is measured by the quartz crystal based on initial calibrations. The rate is then used to calculate the thickness of the film over time.

In general, highly homogenous vanadium oxide thin films with uniform thickness and crystallinity can be grown by the PIAD process [18]. A constant deposition rate leads to a steadily increasing film thickness. Also, the other tracked process parameters, especially the gas flow of the plasma source and discharge current, need to be constant to achieve homogenous films and this was found to be achievable throughout multiple depositions [18].

The present study is dedicated to a deposition (performed at 150°C and V_d of 100 V), where uncontrolled fluctuations of the tracked parameters were observed (Fig. 2). Soon after the start of the deposition,

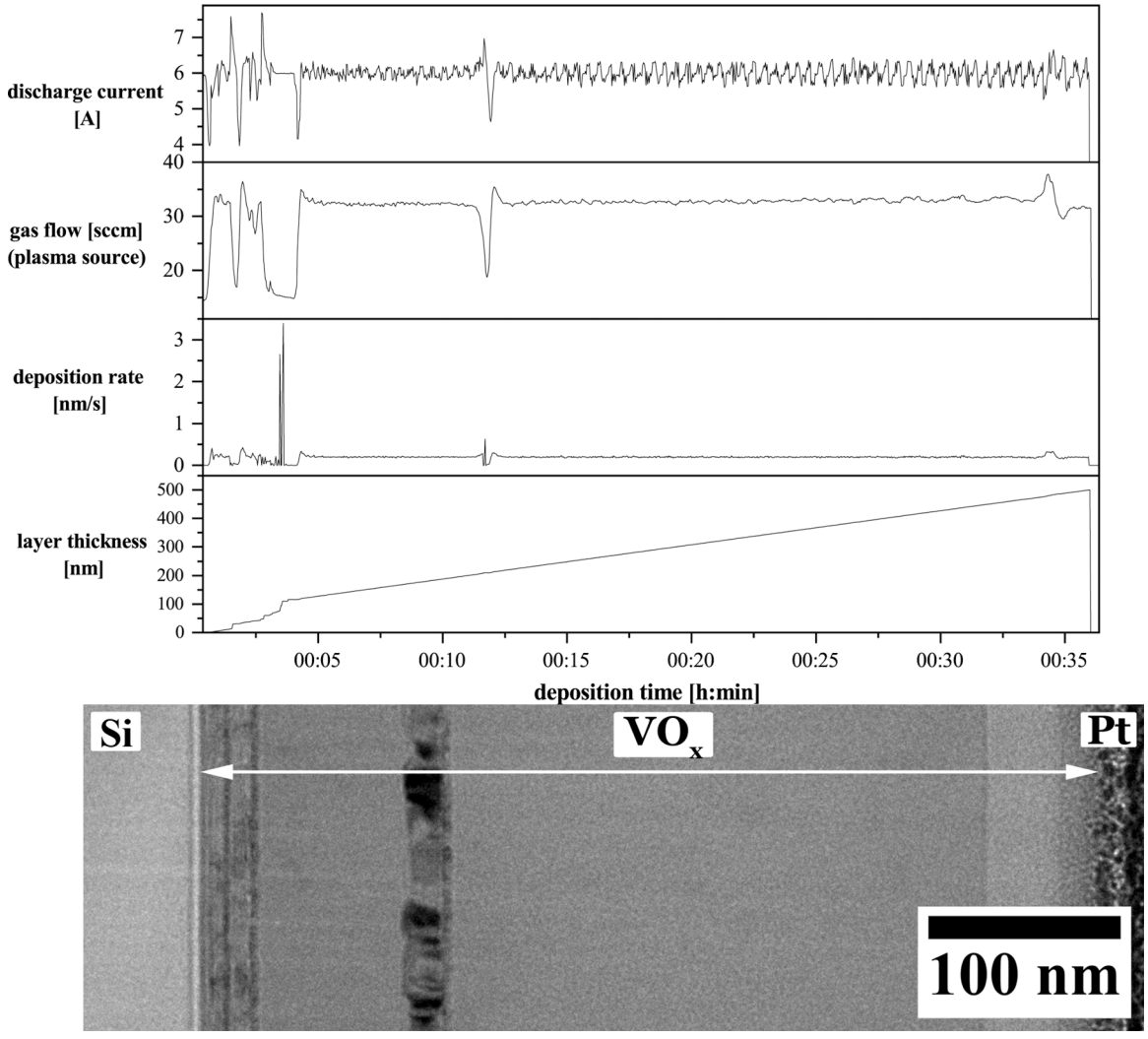

Fig. 2. Comparison between the tracked deposition parameters and a BF TEM image of the VO_x film on Si for the complete deposition process. The deposition time is adjusted according to the complete film thickness, *i.e.* from Si substrate to protective Pt coating.

one can see the heavy fluctuations of both I_d and gas flow. With a closer look, it is evident that a sudden increase in I_d causes the system to react and reduce the gas flow on the plasma source accordingly. The abrupt change in the operating parameters has an impact on the overall pressure inside the chamber and therefore the density of species available for plasma operation and oxidation of the evaporated vanadium metal, as well as an impact in the measured deposition rate. Specifically, an increase in I_d, as observable until ≈12 min deposition time, leads to higher energy fluxes and therefore more ions hitting the substrate per time interval. Accordingly, changes in the microstructure are expected and analyzed in depth in the present work.

The film appears amorphous from GIXRD measurements and only the strong (111) reflection of the Si substrate can be clearly observed (pattern shown in Fig. 3 (a)). The presence of weak reflections around

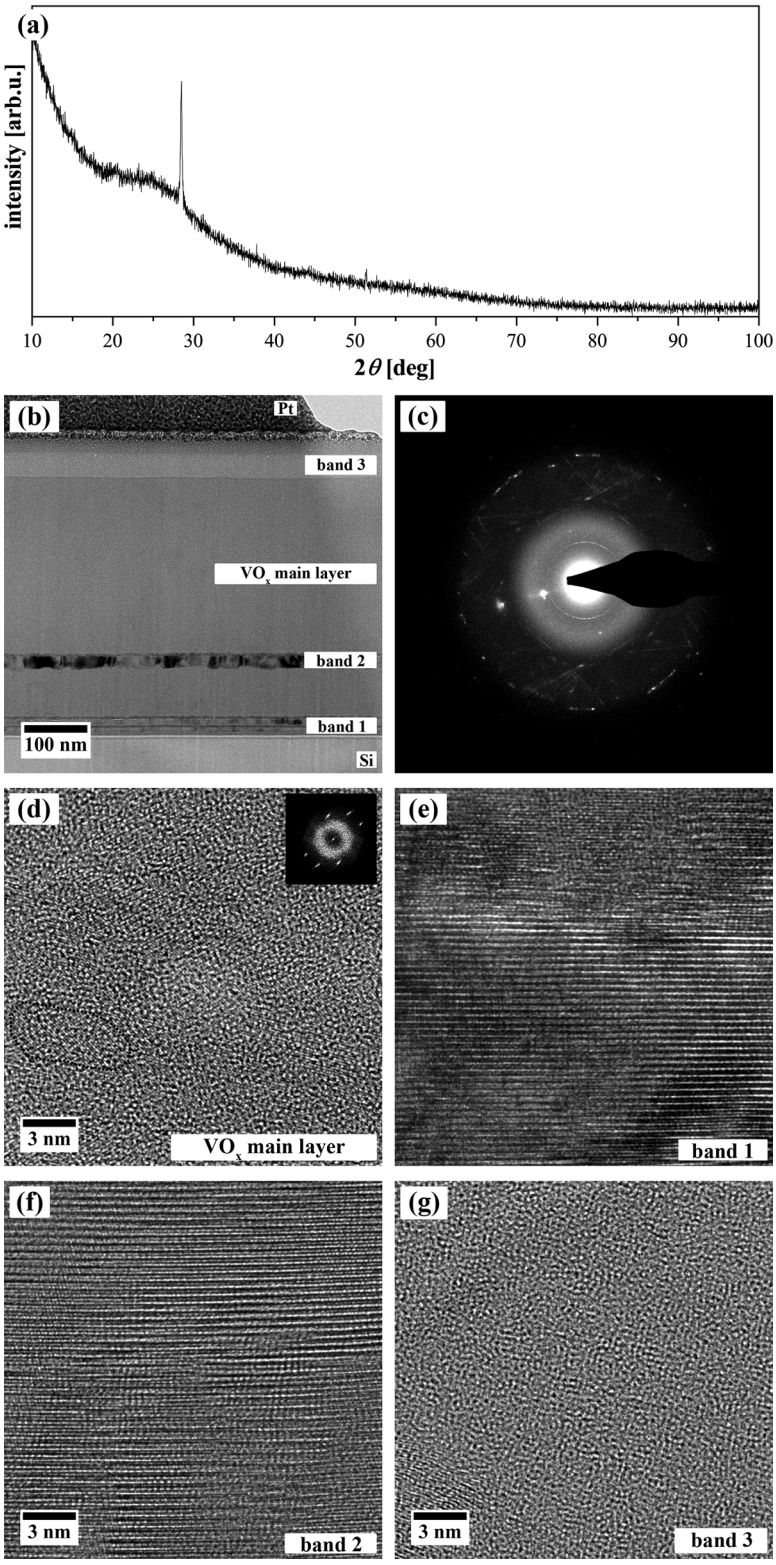

Fig. 3. (a) Grazing incidence XRD diffractogram of a VO_x film on Si, deposited by PIAD at 150°C substrate temperature and 100 V. The strong peak at ≈29° originates from the Si substrate. (b) Cross-sectional BF TEM image of the VO_x film on Si and (c) electron diffraction pattern taken over the whole film. (d) – (g) HR TEM images of the different areas of the film, (d) main layer consisting of nanocrystals surrounded by an amorphous matrix (see FFT as inset), (e) highly crystalline band 1, (f) band 2, and (g) the mainly amorphous, brighter appearing top layer band 3(e).

20° and 45° should be mentioned, however, the noisy pattern did not allow for exact phase analysis. Therefore, TEM investigations were needed to analyze the crystallinity and phase of the as-deposited film in more detail.

TEM measurements on the FIB prepared lamella show a VO_x film with a smooth surface (Figs. 2 and 3) and an overall homogenous thickness of 479±5 nm, in close agreement with the targeted film thickness of 500 nm. The deviation in thickness is likely due to errors during the calibration of the microbalance and, as visible in Fig. 2, fluctuations in the deposition rates. In the bright field (BF) TEM micrograph (Fig. 3 (b)), showing the complete VO_x film on the silicon substrate and the FIB Pt deposition on top, some further contrast variations can be observed within the film. Their appearance correlates with the fluctuations in the deposition parameters, as shown in Fig. 2.

From the TEM investigations, it can be concluded that the main part of the VO_x film consists of nanocrystals surrounded by an amorphous phase, in the following referred to as nanocrystalline part (Fig. 3 (b), (d)). However, in addition, there are highly crystalline bands visible which appear with a darker signal in the BF TEM images and one band with lower brightness. The first contrast variation is appearing close to the Si substrate and consists of one larger band, composed of two smaller crystalline bands (hereafter referred to as band 1), with a total thickness of 24±1 nm. These two smaller bands are caused by two distinct sets of fluctuations in the deposition parameters during the first five minutes of deposition, as can be observed from Fig. 2. The brighter appearing region between the Si substrate and the start of the first crystalline band stems from the native, amorphous substrate oxide, SiO_2, which was not removed before the deposition of VO_x. The second crystalline band is present after 104±1 nm of the VO_x film and has a thickness of 22±2 nm (referred to as band 2). Bands 1 and 2 consist of large crystallites with lengths ranging from 13 up to 66 nm. On top of the film, close to the protective Pt layer, a band with a brighter appearing signal can be observed in the BF TEM images. This band has a thickness of 39±2 nm and is located at an overall film thickness of 424 ± 2 nm and will be referred to as band 3 in the following. A similar contrast variation at the surface of the film was observed for VO_x films deposited with the same deposition parameters (150°C, 100 V) but where no fluctuations occurred [18]. As this layer is mainly amorphous, as also described in the following, it is ascribed to remaining reactants in the chamber shortly after shutting off the process, which are still depositing on top of the film.

The reason why peaks originating from the crystalline bands do not appear clearly in the GIXRD pattern (Fig. 3 (a)) is because grazing incidence geometry was used. While penetrating the sample the primary X-ray beam is already scattered and reaches the crystalline bands 1 and 2 with a lower intensity and gets further weakened when being diffracted and leaving the sample. Additionally, the overall contribution of highly crystalline parts in the presented films is low (thin bands) and the size of the nanocrystals embedded in the mainly amorphous matrix is small. Nanocrystals lead to broad peaks and diffuse, noisy reflections are visible between 20° and 35°, which are overlapped by the intense, broad signal related to the amorphous phase of the thin film. No clear assignment to any phase was possible from these diffuse and noisy reflections.

Electron diffraction patterns taken with a selected area aperture (resulting in an illuminated circular area with a diameter of ≈440 nm) contain contributions from the whole VO_x film. Mainly diffraction rings and a few individual reflections were observed on a large amorphous background (Fig. 3 (c)). This confirms an amorphous phase as the main phase but also the presence of polycrystalline parts besides. As mentioned, the *d*-values of the different possible VO_x phases are very similar and an unambiguous assignment to one single phase cannot be established. Furthermore, some *d*-values are very close to each other, and instead of a sharp reflection rather broad ones occur. Still, some of the values can only be explained by one or two vanadium oxide phases. These values are highlighted bold in Table 1 and will be discussed in the following.

Table 1
Summary of *d*-values extracted from the different diffraction patterns and their comparison to literature values. All values are given in Ångstrom [Å]. Values which can only be explained by one phase are highlighted bold. Smaller *d*-values are not listed as they cannot be used to distinguish the phases.

electron diffraction whole layer	α-V_2O_5 [19]	γ-V_2O_5 [20]	V_4O_9 [21, 25]	V_6O_{13} [21]	VO_2 [22]
4,87	-	5,02	5,04	4,98	-
4,69	-	-	-	4,68	4,70
4,54	-	4,48	4,54	-	-
4,04	4,09	-	4,04	-	-
3,46	-	-	-	3,51	-
3,41	3,41	3,37	3,39	-	3,39
3,34	-	-	3,33	3,32	-
3,12	-	3,17	3,09	-	-
2,98	-	-	2,99	2,96	-

In Table 1 the measured *d*-values of multiple diffraction patterns are summarized and accordingly compared to various possible VO_x phases [17, 19–22]. *d*-values larger than > 5 Å are not detected as they are, due to the chosen camera length, either hidden in the central spot related to overexposure by the primary beam and/or by the beam stopper. Some of the measured *d*-values can only be explained by one or two phases, these are highlighted bold in Table 1. Comparison reveals that these values mainly stem from either V_4O_9 or V_6O_{13} which are both mixed-valence oxides. As the fit of both V_2O_5 modifications is also good it is likely that one (or both) of them are present, especially as the deposition is taking place in a highly oxidizing atmosphere. The presence of V_6O_{13} is especially likely as this phase was confirmed by XRD analysis on similar VO_x films (*i.e.* prepared by the PIAD method but at slightly different temperatures or voltages) that are composed of V_2O_5 and V_6O_{13} [18]. That VO_2 also partly shows a match to the measured *d*-values can have two reasons: as vanadium in VO_2 has a lower oxidation state of +IV than in V_2O_5 (+V), either the oxidation of the vanadium metal was not complete during the deposition, *e.g.* due to the reduction of the gas flow; or the V_2O_5 film got reduced during the TEM investigation due to interaction with the electron beam [23]. The electron beam reduction of V_2O_5 was observed to happen from V_2O_5 over V_4O_9 and V_6O_{13} down to VO_2 until VO [23,24] and could therefore also explain the presence of the mixed-valence oxides. However, the sole presence of the mixed-valence oxides by electron beam reduction is not likely. Another possibility for an underestimation of the V_2O_5 amount could be the loss of oxygen during the electron beam bombardment.

To further analyze the phase of the different crystalline areas of the film nanobeam diffraction was performed. However, the VO_x layer was fast and strongly damaged by the focused electron beam, which possesses high energy and a possible reduction of the material could not be excluded. Instead, HR TEM images were analyzed and only those were considered where no obvious damage occurred. As for the nanobeam diffraction, damage occurred after extensive measurements at very high magnifications, but this could be followed easily. Images with damage have not been used for phase identification.

Fig. 3 (d)-(g) show high resolution (HR) TEM images of the different areas of the film. The largest observable lattice distances in the crystalline band 1 are around 5.8 Å, which fit well to α-V_2O_5 as well as V_6O_{13}, while the largest lattice distance measured from band 2 with 4.4 Å is smaller and corresponds well to α-V_2O_5 or VO_2 [19, 21, 22]. However, most of the vanadium oxides also show large lattice distances, for example, 5.0 Å or 4.5 Å in γ-V_2O_5 and V_4O_9 [20,25]. The similarity of the *d*-values of the phases makes the assignment of certain phases to the measured values complicate, as also measurement errors have to be considered. An HR TEM image of the VO_x main layer between band 2 and 3 is given in Fig. 4 (c). The inset is a fast Fourier transform (FFT) of the whole image, indicating small crystallites embedded in an amorphous matrix. One of these crystallites is marked exemplarily.

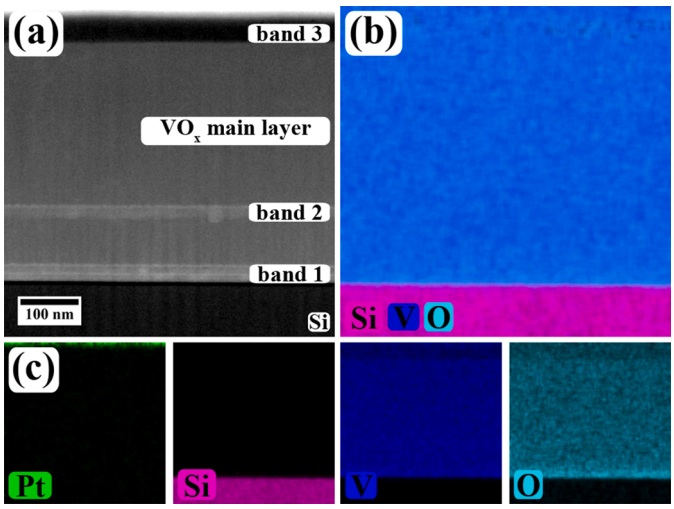

Fig. 4. (a) HAADF STEM image, (b) EDX signal overlay of Si, V, and O signals and (c) single elemental EDX mappings of Pt, Si, V, and O signals, respectively, of the VO_x film.

Measurements on some of these small particles indicate small *d*-values of around 1.9 to 1.8 Å, which unfortunately are lattice distances found similarly in all vanadium oxides discussed here. Finally, an image of the brighter appearing band 3 (Fig. 3 (g)) shows a mainly amorphous layer with a very low amount of nanocrystals. Due to the low amount of nanocrystals a detailed analysis of those was not possible.

High angle annular dark field (HAADF) STEM imaging and EDX measurements were performed to further determine which oxides are formed during the fluctuations of the process parameters. From the HAADF image in Fig. 4 (a) it can be observed that the contrast of the respective bands is reversed compared to the BF TEM images; band 1 and 2 now show a bright contrast while band 3 shows a darker contrast. In HAADF imaging a higher intensity, *i.e.* higher brightness usually means a higher average atomic number *Z* (as the intensity is nearly proportional to Z^2). However, in the presented case the higher brightness in the HAADF STEM image is most likely strongly affected by the remaining diffraction contrast caused by the higher (bands 1 and 2) or respectively lower (band 3) crystallinity of the bands compared to the remaining film. Thus, the image contrast is not directly related to the composition alone.

From the EDX map across the whole film (Fig. 4 (b) signal overlay and (c) single elemental mappings) changes in vanadium content in the bands are not visible. An increasing oxygen signal, though, can be observed for band 1 but close to the silicon substrate. This higher amount of oxygen could either be an indication for a vanadium oxide with vanadium in a higher oxidation state (*i.e.* lower V-to-O ratio) but can also be caused by the amorphous surface oxide, SiO_2, of the substrate. Both vanadium and oxygen signal seem to decrease in the region of band 3; however, this is most likely related to the amorphous nature and accordingly lower atomic packing of the band.

The quantified V-to-O ratios from the different areas of the sample were analyzed with the help of an experimental k-factor. As mentioned before, the received mass ratios were converted to atomic ones. The possible phases V_2O_5, V_4O_9, V_6O_{13}, VO_2, or V_2O_3 have nominal V-to-O ratios of 0.40, 0.44, 0.46, 0.50, 0.67, respectively, which are similar. However, as electron diffraction and HR TEM indicate mixed phases, these values can still give indications if the targeted area contains more or less oxidized phases. The EDX quantification itself is affected by an overlap of the oxygen Kα with the vanadium Lα line at around 0.5 keV. Still, a comparison of the different regions of the film can be done by calculating the V-to-O ratios using the oxygen Kα and the vanadium Lα lines as the systematic error is the same for the different oxides. Also, it has to be mentioned that a loss of oxygen during the illumination with the electron beam can occur as well.

The obtained V-to-O ratio for the nanocrystalline main layer was 0.52 ± 0.02. This value is very close to the V-to-O ratio of VO_2 of 0.50 and gives a strong hint that the main phase of the film is VO_2. Measurements on band 2 resulted in a slightly higher value of 0.57 ± 0.02, which can be also attributed to the presence of VO_2. In contrast, the region of band 1 shows a strongly decreased overall V-to-O ratio of 0.35 ± 0.04, with the measured ratios increasing from the Si substrate towards the top. Close to the substrate the V-to-O ratio of band 1 is 0.28, increasing towards the top of the film from 0.33, 0.36, 0.39, and 0.42 at the end of band 1. It is likely that the amorphous SiO_x between substrate and film partly causes this higher oxygen content. Farther away from the interface the averaged V-to-O ratio becomes 0.39 ± 0.02, corresponding to V_2O_5. Band 3, finally, is giving a V-to-O value of 0.32 ± 0.10. As the standard deviation is high, it could be a V_2O_5 amorphous phase.

However, it has to be mentioned that the observed changes can also be influenced by varying thickness and/or crystallinity within the film, influencing the measurement. For example, channeling conditions can affect quantification. Additionally, an influence of the overlap of O K with V L has to be considered. Furthermore, as mentioned before, a possible influence by reduction of the V_2O_5 in the electron beam cannot be excluded.

Although vanadium oxides showing similar *d*-values, especially in the lower *d*-values (not listed in Table 1 for this reason), which makes diffraction analysis difficult, a clearer picture can be achieved with quantitative EDX analysis (described above). As most vanadium oxides can be nicely differentiated in EELS by their electron energy loss near edge structure (ELNES), associated with each element-specific edge and its oxidation state [10, 11, 26], this method was chosen to gain additional insight into the nature of the VO_x thin film and the influence of the deposition parameters and especially to unravel the oxidation state of vanadium in the film.

Fig. 5 (a) shows the EEL spectra, obtained on the different areas of the film, within an energy loss region from 510 to 550 eV. The spectra are aligned according to their first maximum in the O K edge [27]. The main features of the ELNES in this area are the V $L_{3,2}$ white lines with an onset around 515 eV. Fine spectral features cannot be observed. The white lines are followed by the O K edge with an onset at around 530 eV. However, contrary to spectra published in literature we cannot observe a clear splitting of the O K edge at around 532 eV which would be expected for α-V_2O_5 and most of the other oxides with oxidation state > +IV [10,11]. However, in the spectra of band 1 a shoulder within the O K edge can be seen (Fig. 5, marked by arrow) and such asymmetry of the O K edge can also be observed for the spectra of band 2 and the main film, but not as pronounced. The presence of this shoulder hints on the presence of either α-V_2O_5, V_4O_9, V_6O_{13}, or VO_2, as for the lower oxidized oxides no splitting or shoulder can be observed [10, 11, 23]. However, the presence of only a shoulder instead of a full splitting of peaks of the O K edge was also predicted by theoretical calculations for γ-V_2O_5 [26]. This phase is different from the α-modification only in the octahedral ordering [26]. This difference in the octahedral arrangement/coordination is reflected in the O K fine structure by a loss of the O K split between e_g and t_{2g} by losing the long-range order [11,26]. As the growth of a γ-V_2O_5 phase has been observed before for ion beam sputter deposited thin films [27] we conclude that γ-V_2O_5 could be grown also in the presented case [28]. Although γ-V_2O_5 is a metastable phase which transforms into the α modification at temperatures around 340°C [28], it can grow as our deposition process takes place at only 150°C substrate temperature and no additional annealing step was performed. Of course, a missing shoulder and/or the loss of splitting in the O K edge can also be due to a too low spectral resolution of the EELS measurements or an overlap of different phases. When comparing the obtained O K spectra to published ones, it would also be possible that the present VO_x phase is VO with vanadium in oxidation state +II [11]. Nevertheless, as the deposition of the vanadium oxide films was taking place in a generally highly oxidizing environment we do not assume that such less oxidized

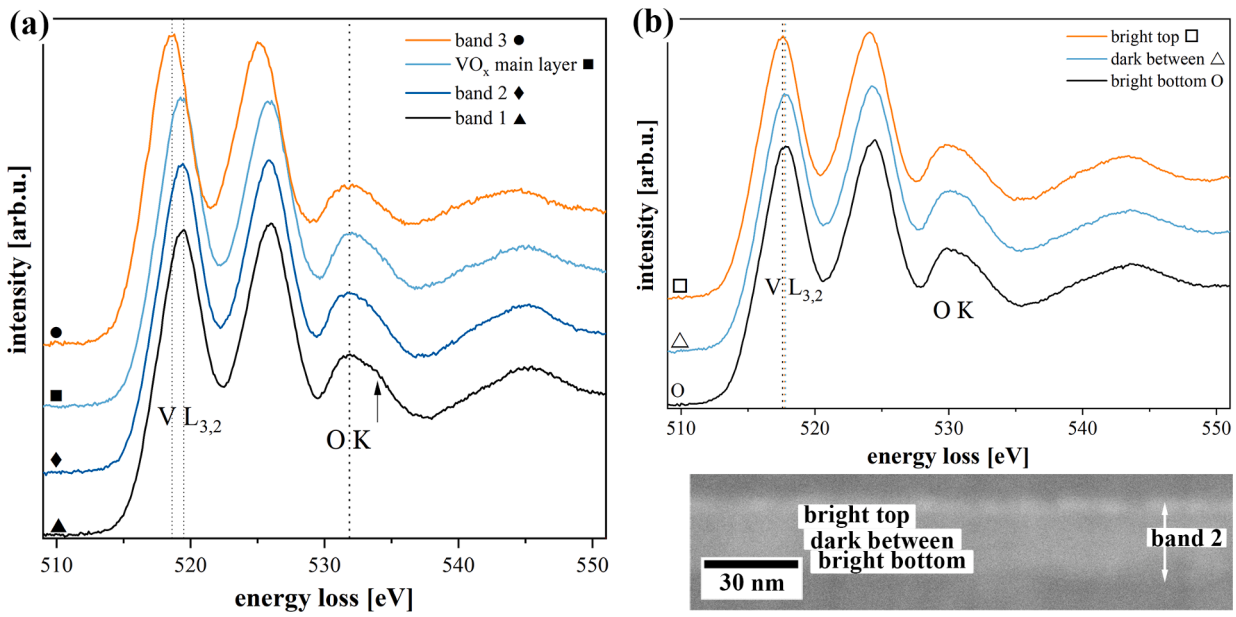

Fig. 5. (a) EEL spectra taken at different locations of the VOx thin film. Each spectrum has been extracted from a mapped area and the spectra have been aligned according to the first maximum of the O K edge[27]. (b) EEL spectra taken at different locations within band 2.

vanadium should be present in a large quantity, even not in the formed bands at the lower oxygen flow in the plasma source. Furthermore, no hints of a VO phase could be found with electron diffraction, HR TEM, and quantitative EDX.

Interestingly, there are no big differences in the fine structure of the O K EELS spectra between crystalline bands 1 and 2 and the remaining film, which gives a hint that the octahedral coordination in the nanocrystalline areas of the VO_x film is already established and comparable to the one in the crystalline bands and therefore represented in the ELNES structure. For the bright band 3, a shift of the V $L_{3,2}$ edge of ≈1.5 eV towards lower energies can be observed. This shift – in respect to the O K edge onset – is an indication for an overall lower vanadium oxidation state as observed by Gallasch et al. [27]. Furthermore, also the intensity ratio between L_3 and L_2 line is changing for band 3 with L_3 becoming more intense, while L_2 is more intense for the bands 1 and 2. A decreasing L_3 intensity also is related to a decrease in the vanadium oxidation state [23,26]. Concluding, a lower vanadium oxidation state could be present in band 3. The fact that the intensity ratio of L_3 and L_2 is nearly equal for the main nanocrystalline layer can give a hint that in the main layer also some lesser oxidized vanadium oxides are present, for example, V_6O_{13}, V_4O_9 (both mixed-valence oxide with V in oxidation states +IV and +V) or VO_2. This fits the XRD pattern of similar grown films where no abrupt parameter change was observed and can also be supported by the electron diffraction data and FFT analysis.

In the HAADF images, bands 1 and 2 appear bright and closer investigation even reveals a layered appearance within, composed of bright and darker stripes (compare Fig. 4 (a) and Fig. 5 (b) bottom). EELS measurements were conducted on the different layers of band 2 and the spectra are shown in Fig. 5 (b). The blue curve (labeled *bright bottom*) marks the onset of band 2, followed by a slightly less intense layer (red curve, labeled *dark between*), and finally a very bright appearing layer (black curve, labeled *bright top*) at the end of band 2. The three spectra all show a very similar shape and only a very slight shift of the V L_3 line of 0.2 eV towards lower energies from the bottom (Fig. 5 (b), black curve) to the top of the band (Fig. 5 (b), orange curve). This indicates a decreasing oxidation state of vanadium within band 2, i.e. an increase of lesser oxidized vanadium oxide compounds. Combined with the results from quantitative EDX measurements, this can indicate the transition from V_2O_5 in the lower part of the film to VO_2 as the main phase in the rest of the film.

Although especially the EELS measurements have been conducted on areas not visibly damaged already, a possible influence of the electron beam reduction during the EELS experiments cannot be excluded and the possible intermediates V_6O_{13} and V_4O_9 in this reduction process have to be included [23,24]. Especially the damage generated during high-resolution TEM and electron diffraction is visible in bright field images after the measurements (not shown). However, for EELS and also EDX measurements there is no strong damage visible afterward.

According to the quantified EDX results the as-deposited film consists of a main phase of VO_2 nanocrystals, embedded within an amorphous matrix, with additional crystalline bands. Band 1 mainly consists of V_2O_5 while band 2 consists of VO_2. This is supported by HR TEM. EELS measurements show a pronounced shoulder in the O K edge for band 1, confirming the presence of V_2O_5. The weakening of this shoulder, as well as a similar intensity in the vanadium L_3 and L_2 white lines, indicate the presence of a less oxidized vanadium oxide for band 2 and the main layer. According to EDX, this phase is VO_2, which is supported by HR TEM. Band 2 is also the transition area between the V_2O_5 and VO_2 phase (Fig. 5). Band 3 reveals contradictory EDX and EELS results. While EDX shows a V_2O_5 phase, EELS reveals a chemical shift and L_3/L_2 intensity ratio which relates to a lower oxidation state than the rest of the film. This can be caused by FIB preparation. The deposition of the protective Pt layer can induce changes in composition and crystal structure of the surface region of the VO_x film, for example by reduction of the material, similar to the effect under the electron beam [23,24]. Thus, band 3 most likely consists of VO_2. Taking into account the results from electron diffraction and HR TEM, also the mixed-valence oxides V_4O_9 and/or V_6O_{13} can be present throughout the whole film alongside the main phases V_2O_5 and VO_2.

A comparison to the tracked deposition parameters reveals a correlation between deposition parameters and the observed crystalline bands. An overview is shown in Fig. 2. The crystalline bands 1 and 2 are related to an increase in the discharge current I_d of the ion source and a respective decrease of the gas flow of the plasma source while a reverse fluctuation of these parameters can be seen for the (in BF TEM) brighter appearing contrast on top of the film (band 3). An increase of I_d can lead to a higher energy flux within the chamber, *i.e.* more ions hitting the surface at the same time, resulting also in an increase of the deposition rate, as can also be observed in Fig. 2. In the presented case, this leads to a denser and more crystalline packing of the ions and thus to the

crystalline bands 1 and 2. However, bands 1 and 2 differ in their vanadium oxide phase. Band 1, the closest one to the substrate, mainly consists of V_2O_5. Band 2, on the other hand, mainly consists of VO_2. This may be caused by a possibly higher temperature closer to the substrate, facilitating the growth of the most stable vanadium oxide, V_2O_5. Farther away from the substrate at a presumably lower temperature, the overall energy seems to be not enough to grow V_2O_5 but sufficent for VO_2 instead. The higher energy flux caused by the increase of I_d only leads to an increased crystallinity, while the decreased oxygen flow can lead to lesser oxidized vanadium oxide phases. For band 3, on the other hand, the lower discharge current led to a lower energy flux and therefore a decreased crystallinity and an amorphous band. Consequently, the phase of this band could also be a lower oxidized vanadium oxide as indicated by EELS. However, an exact assignment is complicated due to possible sample preparation damage to the upper areas of the film. Furthermore, at the beginning of the deposition, the tracked film thickness gives an uneven increase, at one point even an abrupt step, which also hints at varying growth rates. This step in nominal/measured film thickness can also explain the deviation of the tracked film thickness in comparison to the achieved thickness as measured by TEM, *i.e.* due to the step the tracked film thickness is always a little higher than the real deposited one. It further explains why bands 2 and 3 seem to appear at higher thicknesses (tracked film thickness vs. variations in the parameters) than observed in the sample itself.

To summarize, this work gives proof that a rapid change of deposition conditions, in the present case an unintentional change of the discharge current of the plasma source, strongly influences the degree of crystallinity of VO_x films on silicon substrates. A high crystallinity/large grains can be observed with a sudden increase of discharge current because of a higher density of ions reaching the film surface at a time. The respective decrease in oxygen flow can lead to higher amounts of lesser oxidized vanadium oxide species during the deposition. On the other hand, a sudden unintentional decrease of I_d, which leads to an increase in oxygen flow and fewer ions hitting the film surface as described above, can lead to amorphous films. In the presented case, the variations in discharge current were most likely caused by the inhomogeneous melting of the target material. However, the modification of the phase does not seem to be strongly influenced and seems to be more an effect of overall energy. Close to the substrate and therefore at the highest temperature, V_2O_5 is grown. With increasing film thickness, the crystalline phase evolves to VO_2, as electron diffraction as well as EELS investigations and STEM EDX measurements prove. It has to be mentioned that difficulties in the analysis, *e.g.* remaining diffraction contrast in HAADF STEM imaging, an overlap of V and O edges in EDX and EELS, the closeness of *d*-values for diffraction, and, importantly to already happening beam damage during the measurements, as V_2O_5 is known to become easily reduced in the electron beam, can influence the results. Although no unambiguous assignment can be drawn, it is concluded that the as-deposited VO_x film is consisting of a band of V_2O_5, in the α- as well as in the slightly distorted γ-modification, followed by a main phase of VO_2, partly grown in a crystalline band due to a higher deposition rate, but mainly as nanocrystals embedded within an amorphous matrix. Present alongside, the mixed-valence vanadium oxides V_4O_9 and V_6O_{13}, cannot be excluded. The same phase composition was also observed for a VO_x film, deposited with PIAD at the deposition conditions as presented here, but without the here observed fluctuations in the deposition conditions [18]. The observed fluctuations in the deposition lead to locally enhanced crystal growth by a higher density of ions hitting the surface. While in band 1, close to the substrate, also the temperature is highest, the available energy was enough to grow a VO_x film with a higher content of V^{+5}, while for band 2, with a lower temperature, the amount of lesser oxidized phases is higher. However, as possible beam damage, *i.e.* reduction of V_2O_5 during the (S)TEM measurements, cannot be fully excluded with certainty and additional experiments at lower acceleration voltage will be performed in future to prove this.

4. Conclusion

The presented work gives insights that on-line monitoring of (plasma assisted) deposition parameters is important to link them with properties and/or characteristics of the deposited material. In this study, unintentional changes of the discharge current were identified to be responsible for a change in crystallinity and phase composition. Overall, the film is composed of a mixture of different vanadium oxides, *i.e.* VO_2, V_6O_{13}, V_4O_9, and V_2O_5. Highly crystalline bands were formed with an enhanced discharge current which resulted in a higher density of available ions. Close to the substrate, this resulted in V_2O_5, while further away the amount of mixed-valence oxides and VO_2 is higher. Decreasing the discharge current, on the other hand, led to an amorphous band in the deposited film which is most likely also composed of mainly VO_2. The achieved results indicate that the chosen conditions for this deposition are not suitable to deposit pure V_2O_5 films with vanadium oxidized to the highest and most stable oxidation state and high crystallinity, but rather yield a mixture of (mixed-valence) vanadium oxides. Fluctuations in the discharge current and gas flow then resulted in a change of the deposition conditions suitable for the growth of high crystallinity layers. However, these findings open up future pathways to directly influence the growth of thin films by adjusting different deposition parameters in a direct and traceable way. Monitoring and controlling the deposition parameters will in future allow growing multilayer films with varying crystalline layers which can be suitable for different applications. Influencing the crystalline modification is very important for applications such as water splitting, as these can also directly determine the activity of the material.

CRediT authorship contribution statement

Anna Frank: Conceptualization, Data curtion, Formal analysis, Investigation, Methodology, Writing – original draft, Writing – review & editing. **Miguel Dias:** Data curtion, Formal analysis, Methodology, Writing – review & editing. **Stefan Hieke:** Conceptualization, Formal analysis, Writing – review & editing. **Angela Kruth:** Funding acquisition, Formal analysis, Writing – review & editing. **Christina Scheu:** Conceptualization, Funding acquisition, Formal analysis, Methodology, Supervision, Writing – review & editing.

Declaration of Competing Interest

The authors declare that they have no known competing financial interests or personal relationships that could have appeared to influence the work reported in this paper.

Acknowledgments

The Leibniz Association is gratefully acknowledged for funding of this work as part of the CarMON (carbon metal-oxide nano hybrids) project (SAW- 2017).

References

[1] S. Fleischmann, D. Leistenschneider, V. Lemkova, B. Krüner, M. Zeiger, L. Borchardt, V. Presser, Tailored mesoporous carbon/vanadium pentoxide hybrid electrodes for high power pseudocapacitive lithium and sodium intercalation, Chem. Mater. 29 (2017) 8653–8662.
[2] N.A. Chernova, M. Roppolo, A.C. Dillon, M.S. Whittingham, Layered vanadium and molybdenum oxides: batteries and electrochromics, J. Mater. Chem. 19 (2009) 2526–2552.
[3] W. Luo, J.-J. Gaumet, L. Mai, Nanostructured layered vanadium oxide as cathode for high-performance sodium-ion batteries: a perspective, MRS Commun. 7 (2017) 152–165.
[4] P.Y. Zavalij, M.S. Whittingham, Structural chemistry of vanadium oxides with open frameworks, Acta Crystallogr. Sec. B 55 (1999) 627–663.
[5] R. Abazari, S. Sanati, L.A. Saghatforoush, Non-aggregated divanadium pentoxide nanoparticles: a one-step facile synthesis. Morphological, structural,

compositional, optical properties and photocatalytic activities, Chem. Eng. J. 236 (2014) 82–90.
[6] M.K. Chine, F. Sediri, N. Gharbi, Solvothermal synthesis of V_4O_9 flake-like morphology and its photocatalytic application in the degradation of methylene blue, Mater. Res. Bull. 47 (2012) 3422–3426.
[7] J. Wu, D. Qiu, H. Zhang, H. Cao, W. Wang, Z. Liu, T. Tian, L. Liang, J. Gao, F. Zhuge, Flexible electrochromic V_2O_5 thin films with ultrahigh coloration efficiency on graphene electrodes, J. Electrochem. Soc. 165 (5) (2018) D183–D189, https://doi.org/10.1149/2.0481805jes.
[8] G. Cliff, G.W. Lorimer, The quantitative analysis of thin specimens, J. Microsc. 103 (1975) 203–207.
[9] D.B. Williams, C.B. Carter, Transmission Electron Microscopy, Second ed., Science +Business Media, New York, 2009.
[10] L. Laffont, M.Y. Wu, F. Chevallier, P. Poizot, M. Morcrette, J.M. Tarascon, High resolution EELS of Cu–V oxides: application to batteries materials, Micron 37 (2006) 459–464.
[11] C. Hébert, M. Willinger, D.S. Su, P. Pongratz, P. Schattschneider, R. Schlögl, Oxygen K-edge in vanadium oxides: simulations and experiments, Eur. Phys. J. B - Condens. Matter Complex Syst. 28 (2002) 407–414.
[12] H.R. Kaufman, R.S. Robinson, R.I. Seddon, End-Hall ion source, J. Vacuum Sci. Technol. A 5 (1987) 2081–2084.
[13] L.A. Giannuzzi, F.A. Stevie, A review of focused ion beam milling techniques For TEM specimen preparation, Micron 30 (1999) 197–204.
[14] S.W. Hieke, G. Dehm, C. Scheu, Annealing induced void formation in epitaxial Al thin films on sapphire (α-Al_2O_3), Acta Mater. 140 (2017) 355–365.
[15] M. Baram, W.D. Kaplan, Quantitative HRTEM analysis of FIB prepared specimens, J. Microsc. 232 (2008) 395–405.
[16] M. Schaffer, B. Schaffer, Q. Ramasse, Sample Preparation for atomic-resolution STEM at low voltages by FIB, Ultramicroscopy 114 (2012) 62–71.
[17] R.W.G. Wyckoff, Crystal Structures, Second ed., 1, Interscience Publishers, New York, New York, 1963.
[18] M. Dias, A. Frank, J. Harhausen, C. Scheu, R. Brandenburg, A. Kruth, Correlation between ion energy distribution and structural properties of VxOy layers in an near-industrial plasma ion-assisted deposition process, under review, (2021).
[19] R. Haberkorn, J. Bauer, G. Kickelbick, Chemical Sodiation of V_2O_5 by Na_2S, Zeitschrift für anorganische und allgemeine Chemie 640 (2014) 3197–3202.
[20] M. Safrany Renard, N. Emery, E.M. Roginskii, R. Baddour-Hadjean, J.-P. Pereira-Ramos, Crystal structure determination of a new sodium vanadium bronze electrochemically formed, J. Solid State Chem. 254 (2017) 62–68.
[21] K.-A. Wilhelmi, K. Waltersson, L. Kihlborg, A refinement of the crystal structure of V_6O_{13}, Acta Chem. Scand. 25 (1971) 2675–2687.
[22] H.T. Evans Jr., M.E. Mrose, A crystal chemical study of montroseite and paramontroseite*, Am. Mineral. 40 (1955) 861–875.
[23] D.S. Su, M. Wieske, E. Beckmann, A. Blume, G. Mestl, R. Schlögl, Electron beam induced reduction of V_2O_5 studied by analytical electron microscopy, Catal. Lett. 75 (2001) 81–86.
[24] H.J. Fan, L.D. Marks, Phase transitions in V_2O_5 in a high resolution electron microscope, Ultramicroscopy 31 (1989) 357–364.
[25] K.-A. Wilhelmi, K. Waltersson, On the crystal structure of a new vanadium oxide, V_4O, Acta Chem. Scand. 24 (1970) 3409–3411.
[26] M. Willinger, N. Pinna, D.S. Su, R. Schlögl, Geometric and electronic structure of γ-V_2O_5: comparison between α-V_2O_5 and γ-V_2O_5, Phys. Rev. B 69 (2004), 155114, https://doi.org/10.1103/PhysRevB.69.155114.
[27] T. Gallasch, T. Stockhoff, D. Baither, G. Schmitz, Ion beam sputter deposition of V_2O_5 thin films, J. Power Sources 196 (2011) 428–435.
[28] J.M. Cocciantelli, P. Gravereau, J.P. Doumerc, M. Pouchard, P. Hagenmuller, On the preparation and characterization of a new polymorph of V_2O_5, J. Solid State Chem. 93 (1991) 497–502.